Materials Letters 275 (2020) 128165

Contents lists available at ScienceDirect

Materials Letters

journal homepage: www.elsevier.com/locate/mlblue

Rapid microwave-assisted hydrothermal synthesis of $CuBi_2O_4$ and its application for the artificial photosynthesis

Lucas S. Ribeiro [b], Ivo M. Pinatti [b], Juliana A. Torres [c], Amanda S. Giroto [c], Fabiana Lesse [a], Elson Longo [b], Caue Ribeiro [c], André E. Nogueira [a,*]

[a] Department of Chemistry, Institute of Exact and Biological Sciences (ICEB), Federal University of Ouro Preto-UFOP, Zip Code 35400-000, Ouro Preto, Minas Gerais, Brazil
[b] Interdisciplinary Laboratory of Electrochemistry and Ceramics (LIEC), Departament of Chemistry, UFSCar-Federal University of São Carlos, Rod.Washington Luis km 235, CP 676 São Carlos, SP 13565-905, Brazil
[c] Embrapa Instrumentation, Rua XV de Novembro, 1452, CEP: 13560-970, CP 741, São Carlos, SP, Brazil

ARTICLE INFO

Article history:
Received 6 April 2020
Received in revised form 12 June 2020
Accepted 14 June 2020
Available online 15 June 2020

Keywords:
CO_2 photoreduction
Copper bismuthate
Microwave-assisted hydrothermal synthesis
Photocatalysis
Morphology

ABSTRACT

Strategies for CO_2 reforming for hydrocarbon production using ultraviolet or visible radiation are promising to mitigate environmental impacts from other human activities. Semiconductors act as photocatalysts for light-to-fuel conversion, but a rigorous control of their structure and morphology is crucial for high efficiency and selectivity. Thus, $CuBi_2O_4$ semiconductors have been synthesized by the microwave-assisted hydrothermal method and studied for the CO_2 photoreduction process. This method produced crystalline materials with controlled morphology using low temperatures and short processing time. Moreover, the semiconductors showed excellent catalytic performance and selectivity, approximately 90% in the conversion of CO_2 to CH_4. Therefore, our new synthesis approach was adequate for $CuBi_2O_4$ preparation, providing an essential indication of activity in the CO_2 photoreduction process.

1. Introduction

The increasing consumption of energy from fossil fuels and the raise in atmospheric carbon dioxide levels has raised considerable concerns about its effects on the climate and energy future. As a result, research to minimize the pollutant loads and to replace fossil fuels for cleaner sources has increased [1,2].

The "artificial photosynthesis," i.e., photocatalytic processes to convert greenhouse gases to hydrocarbons, is under intense investigation for these purposes [3]. In-depth studies toward catalysts for these reactions are still needed to make them viable and energetically favorable, e.g., by activating them through solar radiation [4,5]. In this way, $CuBi_2O_4$ is a promising semiconductor with a bandgap energy value of 1.8 eV, excellent response to visible light, photostability, and the required band potential to reduce CO_2 [6–9].

Furthermore, the activity of the photocatalysts depends not only on the intrinsic physical properties but also relates to the size, morphology, and defects of the particles, as well as other surface properties. These extrinsic properties can be modified by changing the preparation and reaction conditions [10–13].

Microwave-assisted hydrothermal synthesis is efficient in controlling morphology due to its advantages in facilitating crystal growth with low processing time and temperature [14,15]. Thus, we synthesized $CuBi_2O_4$ nanoparticles through microwave-assisted hydrothermal synthesis using different times, aiming to observe the growth mechanisms and their influence on the catalyst activity for CO_2 photoreduction.

2. Materials and methods

2.1. Microwave-assisted hydrothermal synthesis of $CuBi_2O_4$

The $CuBi_2O_4$ nanoparticles were synthesized by mixing 20 mL of a 0.03 M solution of Bismuth (III) nitrate pentahydrate (98%, Synth), 3 mL of HNO_3 and 20 mL of 0.015 M solution of Copper (II) nitrate trihydrate (98%, Synth) under constant magnetic stirring until complete solubilization. After that, 60 mL of 1.25 M solution of NaOH was added to the capsule which was then autoclaved. The microwave treatment was performed at 100 °C for 8, 16 and 32 min. After the reaction, the autoclave was naturally cooled to

* Corresponding author.
E-mail address: andre.esteves@ufop.edu.br (A.E. Nogueira).

https://doi.org/10.1016/j.matlet.2020.128165
0167-577X/

room temperature. The product was recovered by centrifugation, washed twice in water, and then dried in air at 60 °C for 12 h.

2.2. Characterization

The $CuBi_2O_4$ powder was characterized by X-ray diffraction (XRD), using CuKα radiation with λ = 0.15406 nm, employing a Shimadzu XRD 6000 diffractometer. Raman spectra were obtained with a Horiba Jobin-Yvon Raman micro-spectrometer LabRAM at room temperature using the 633 nm line of a 5.9 mW He–Ne laser as the excitation source through an Olympus TM BX41 microscope. The morphologies of the materials were characterized by field emission scanning electron microscopy (FESEM), using a JSM 6701F microscope (JEOL) operated at 5 kV. Diffuse reflectance spectra (DRS) at room temperature, using a Cary 5G instrument (Varian) operated in diffuse reflectance mode.

2.3. CO_2 photoreduction

The CO_2 photoreduction reactions were carried in a 240 mL capacity cylindrical steel reactor, covered with borosilicate glass under UVC light (PHILIPS 5 W), with a maximum wavelength intensity of 253.7 nm. Fig. S1 shows a demonstrative picture of CO_2 photoreactor. 100 mg of the catalysts were dispersed in 100 mL of distilled water and kept under constant stirring. Before starting the reaction, high purity CO_2 was bubbled for 20 min to saturate the reactor, ensuring the elimination of all dissolved oxygen. Experimental details concerning the CO_2 photoreduction process are available in the supplementary material.

3. Results and discussion

The X-ray diffraction (XRD) patterns and Raman spectra of the $CuBi_2O_4$ synthesized at different times (8 min, 16 min, and 32 min) are shown in Fig. 1. All the diffraction peaks for $CuBi_2O_4$ can be indexed according to the standard diffraction pattern (JCPDS File N°. 72–0493), implying that the particles crystallize into single $CuBi_2O_4$ tetragonal phase [16]. The patterns show that no structural change is perceptible at different times (Fig. 1a). However, the precipitated precursor has an amorphous feature.

Fig. 1b shows the evolution of $CuBi_2O_4$ Raman spectra with the synthesis time at 100 °C. The Raman spectra showed six bands centered at 128, 186, 258, 404, 464 and 586 cm^{-1} related to the $CuBi_2O_4$ tetragonal structure. The present Raman analysis is consistent with the recent work reported by Yuvaraj et al., in which $CuBi_2O_4$ has been synthesized by the hydrothermal route [17]. The peak at 128 cm^{-1} refers to the A_{1g} mode, from translational vibrations of the CuO_4 planes along the z axis. The band at 186 cm^{-1} is attributed to the E_g mode related to the vibration of Cu-Cu. The mode A_{1g} centered at 258 cm^{-1} corresponds to the rotation of two stacked CuO_4 squares in opposite directions. The bands at 404 and 586 cm^{-1} are ascribed to the A_{1g} mode of the Bi–O stretching vibration and breathing of CuO_4 squares respectively.

The optical properties were studied by diffuse reflectance spectroscopy and the bandgap energy was calculated using the Tauc model (See supplementary material Fig.S2) [18]. Bandgap values show that the energies required to excite CBO-8 min and CBO-16 min are quite similar. The values for the CBO-8 min, CBO-16 min and CBO-32 min were approximately 1.68, 1.71 and 1.80 eV, respectively. Therefore, the differences are minimal, denoting similar electronic property among materials.

In order to explore the morphological evolution of $CuBi_2O_4$, we conducted three experiments varying the synthesis time and keeping other conditions constant. The SEM images of $CuBi_2O_4$ nanoparticles hydrothermally treated at 100 °C are shown in Fig. 2a. The FESEM images show that the morphological transformation is not associated with phase change after microwave-assisted hydrothermal treatment at different times, as shown in the X-ray diffractogram. The material treated for 8 min presents a predominance of coral-shaped particles, and with longer treatment time, these particles become spheres composed of nanorods. The particle size of the material was modified with the synthesis time, presenting an average size of 0.55 μm, 0.95 μm and 5.5 μm for the materials CBO-8 min, CBO-16 min and CBO-32 min respectively (Fig. S3). However, the hydrothermal treatment for 16 and 32 min does not result in a significant change in morphology.

Fig. 2b shows a schematic representation of the proposed self-assembly mechanism of CBO formation and growth. The initial stage of its synthesis occurs with the dissolution of $Cu(NO_3)_2{\cdot}3H_2O$ and $Bi(NO_3)_3{\cdot}5H_2O$, which undergoes a hydrolysis process with NaOH, forming an amorphous green precipitate of $Cu(OH)_2$ and $Bi(OH)_3$. The microwave radiation used in the system promotes vibrations in the charged particles accelerating the dehydration process and the consequent CBO formation. Moreover, the increase in effective collisions between CBO particles caused by microwave radiation promotes rapid growth in high atomic density and thermodynamically favorable crystallographic planes.

The activity of the materials was verified in the CO_2 photoreduction process in aqueous medium (Fig. 3). The semiconductors synthesized showed higher selectivity for CH_4 production (Table 1 However, CO production is favored in longer synthesis time, i.e., CBO-32 min yielded approximately 13.5 μmol.g^{-1} CO after 24 h,

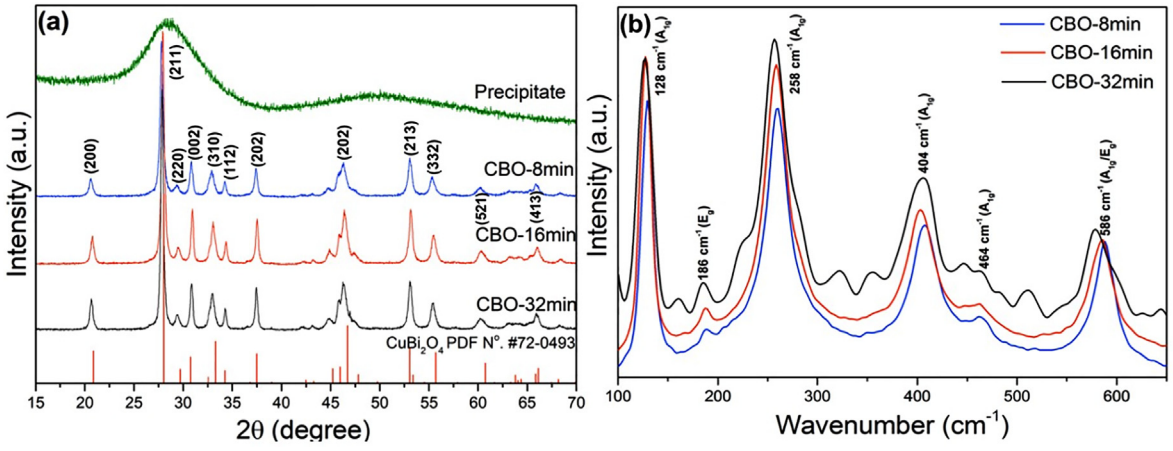

Fig. 1. XRD patterns (a) and Raman spectra (b) of $CuBi_2O_4$ synthesized at different times.

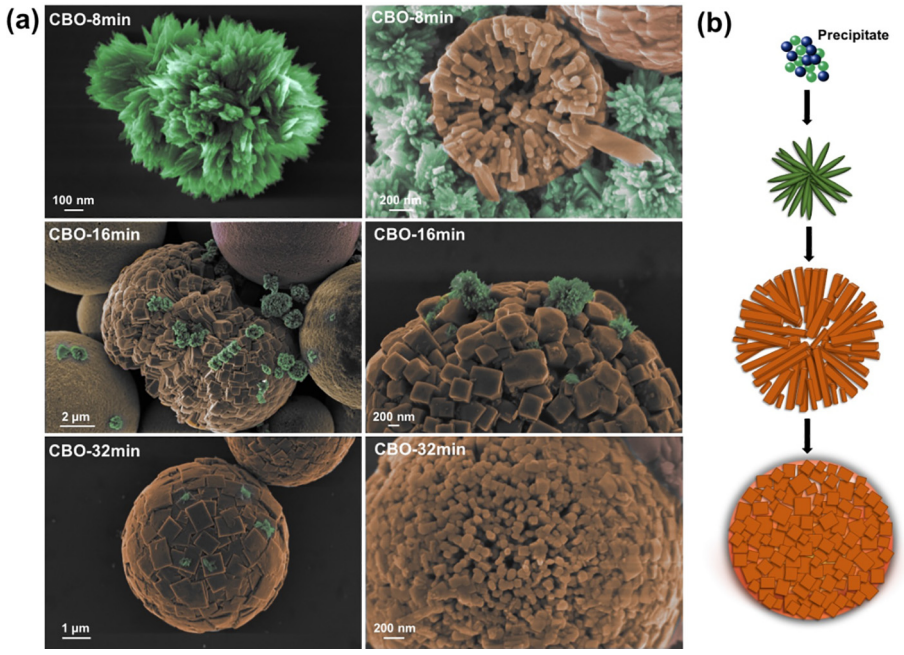

Fig 2. FESEM micrographs of CBO at different times of synthesis (a) and Schematic representation of the nucleation and growth of nanoparticles (b).

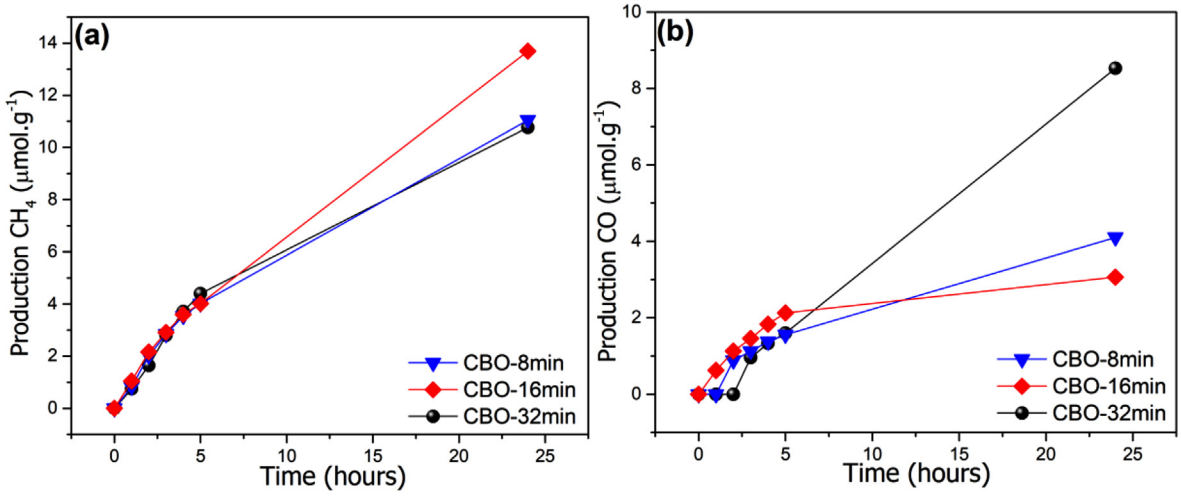

Fig. 3. Kinetics of CH_4 (a) and CO (b) generation from the CO_2 photoreduction under UV irradiation at 25 ± 3 °C.

Table 1
Parameters of the activity of the materials in the CO_2 photoreduction process after 24 h of reaction.

Materials	CO (μmol.g^{-1})	CH_4 (μmol.g^{-1})	*n_{e-} (μmol.g^{-1})	CH_4 selectivity	CO selectivity
CBO-8 min	4.2	11.0	96.4	91.3%	8.7%
CBO-16 min	3.1	13.6	115.0	94.6%	5.4%
CBO-32 min	8.6	10.8	103.6	83.4%	13.6%

* number of electrons involved in CO_2 photoreduction (see supplementary material) into CO and CH_4.
**selectivity was calculated based on electron transfer number involved in CO_2 photoreduction

twice of CBO-8 min and CBO-16 min. Analysis of the liquid phase by NMR indicated acetone and isopropanol in all reactions, which have higher economic values and energy densities than C1 compounds (see supplementary material) [19]. Compared to C1, obtaining C2 and C3 is more challenging due to the high stability of CO_2 molecule, and the high energy barrier for C–C bond formation. Further experiments about the quantification and optimization of the semiconductor ($CuBi_2O_4$) to obtain these products are under discussion.

4. Conclusion

A fast and straightforward microwave-assisted hydrothermal route has been reported for the synthesis of $CuBi_2O_4$ with strict control of semiconductor structure and morphology. The materials exhibited excellent activities in the CO_2 photoreduction process, with a selectivity of approximately 90% in the conversion of CO_2 to CH_4. The results demonstrate a new strategy for quick and easy

synthesis to obtain $CuBi_2O_4$, providing an essential indication of activity in the CO_2 photoreduction process.

CRediT authorship contribution statement

Lucas S. Ribeiro: Conceptualization, Methodology, Investigation, Visualization, Formal analysis, Writing - original draft. **Ivo M. Pinatti:** Methodology, Formal analysis. **Juliana A. Torres:** Formal analysis, Writing - review & editing. **Amanda S. Giroto:** Formal analysis, Writing - review & editing. **Fabiana Lesse:** . **Elson Longo:** Resources, Writing - review & editing. **Caue Ribeiro:** Resources, Writing - review & editing. **André E. Nogueira:** Conceptualization, Writing - review & editing, Supervision.

Declaration of Competing Interest

The authors declare that they have no known competing financial interests or personal relationships that could have appeared to influence the work reported in this paper.

Acknowledgments

The authors would like to thank the financial support provided by Federal University of Ouro Preto - UFOP (Grant #23109.004080/2019-88), São Paulo Research Foundation-FAPESP (Grant #2019/03722-3, #2018/01258-5, #2018/12871-0, #2018/10104-1, #2016/21515-7 and #2013/07296-2), and Embrapa AgroNano research network. The laboratory facilities of LNNA/Embrapa (SISNano Laboratory) are also acknowledged.

Appendix A. Supplementary data

Supplementary data to this article can be found online at https://doi.org/10.1016/j.matlet.2020.128165.

References

[1] B. Han, J. Song, S. Liang, W. Chen, H. Deng, X. Ou, Y.-J. Xu, Z. Lin, Appl. Catal. B-Environ. 260 (2020) 118208.
[2] M. Li, M. Wang, L. Zhu, Y. Li, Z. Yan, Z. Shen, X. Cao, Appl. Catal. B-Environ. 231 (2018) 269–276.
[3] X. Fang, Z. Gao, H. Lu, Z. Zhang, Catal. Commun. 125 (2019) 48–51.
[4] D. Spasiano, R. Marotta, S. Malato, P. Fernandez-Ibañez, I. Di Somma, Appl. Catal. B-Environ. 170–171 (2015) 90–123.
[5] W. Shi, F. Guo, M. Li, Y. Shi, M. Wu, Y. Tang, J. Alloy. Compd. 775 (2019) 511–517.
[6] J. Yang, C. Du, Y. Wen, Z. Zhang, K. Cho, R. Chen, B. Shan, Int. J. Hydrogen Energ. 43 (2018) 9549–9557.
[7] T. Arai, M. Yanagida, Y. Konishi, Y. Iwasaki, H. Sugihara, K. Sayama, J. Phys. Chem. C. 111 (2007) 7574–7577.
[8] F. Guo, W. Shi, H. Wang, M. Han, W. Guan, H. Huang, Y. Liu, Z. Kang, J. Hazard. Mater. 349 (2018) 111–118.
[9] W. Shi, M. Li, X. Huang, H. Ren, F. Guo, Y. Tang, C. Lu, Chem. Eng. J. 394 (2020) 125009.
[10] Y. Zhang, Y. Xie, J. Li, G. Yang, T. Bai, J. Wang, J. Alloy. Compd. 580 (2013) 172–175.
[11] A.E. Nogueira, T.C. Ramalho, L.C.A Oliveira, Top. Catal. 54 (2011) 01-07.
[12] A.E. Nogueira, J.A. Oliveira, G.T.S.T. Silva, C. Ribeiro, Sci. Rep. 9 (2019) 1–11.
[13] F.P. Cardoso, A.E. Nogueira, P.S.O. Patrício, L.C.A. Oliveira, J. Braz. Chem. Soc. 23 (2012) 702–709.
[14] R.K. Singh, R. Kumar, D.P. Singh, R. Savu, S.A. Moshkalev, Mater. Today Chem. 12 (2019) 282–314.
[15] A. Mirzaei, G. Neri, Sensor. Actuat. B-Chem. 237 (2016) 749–775.
[16] F. Guo, M. Li, H. Ren, X. Huang, W. Hou, C. Wang, W. Shi, C. Lu, Appl. Surf. Sci. 491 (2019) 88–94.
[17] S. Yuvaraj, K. Karthikeyan, D. Kalpana, Y.S. Lee, R.K. Selvan, J. Colloid Interf. Sci. 469 (2016) 47–56.
[18] R. Rosei, D.W. Lynch, Phys. Rev. B 5 (1972) 3883–3894.
[19] T. Chatterjee, E. Boutin, M. Robert, Dalton T. 49 (2020) 4257–4265.